



Article

Experimental Verification of a Compressor Drive Simulation Model to Minimize Dangerous Vibrations

Marek Moravič ¹, Daniela Marasová ^{1,*}, Peter Kaššay ², Maksymilian Ozdoba ³, František Lopot ⁴ and Piotr Bortnowski ³

¹ Faculty of Mining, Ecology, Process Control and Geotechnology, Technical University of Kosice, Letna 1/9, 042 00 Kosice, Slovakia; marek.moravic@tuke.sk

² Faculty of Mechanical Engineering, Technical University of Kosice, Letna 1/9, 042 00 Kosice, Slovakia; peter.kassay@tuke.sk

³ Faculty of Geoengineering, Mining and Geology, Wrocław University of Science and Technology, Na Grobli 15, 50-421 Wrocław, Poland; maksymilian.ozdoba@pwr.edu.pl (M.O.); piotr.bortnowski@pwr.edu.pl (P.B.)

⁴ Faculty of Mechanical Engineering, Czech Technical University in Prague, Technická 4, 160 00 Prague, Czech Republic; frantisek.lopot@fs.cvut.cz

* Correspondence: daniela.marasova@tuke.sk; Tel.: +421-55-602-2591

Abstract: The article highlights the importance of analytical computational models of torsionally oscillating systems and their simulation for estimating the lowest resonance frequencies. It also identifies the pitfalls of the application of these models in terms of the accuracy of their outputs. The aim of the paper is to control the dangerous vibration of a mechanical system actuator using a pneumatic elastic coupling using different approaches such as analytical calculations, experimental measurement results, and simulation models. Based on the known mechanical properties of the laboratory system, its dynamic model in the form of a twelve-mass chain torsionally oscillating mechanical system is developed. Subsequently, the model is reduced to a two-mass system using the method of partial frequencies according to Rivin. The total load torque of the piston compressor under fault-free and fault conditions is simulated to obtain the amplitudes and phases of the harmonic components of the dynamic torque. After calculating the natural frequency and the natural shape of the oscillation, the Campbell diagram is processed to determine the critical revolutions. There is a pneumatic flexible coupling between the rotating masses, which changes the dynamic torsional stiffness. The dynamic torque curves transmitted by the coupling are compared with different dynamic torsional stiffnesses during steady-state operation and one cylinder failure. The monitored values are the position of the critical revolutions, the natural frequency, the natural shape of the oscillation, and the RMS of the dynamic load torque. The experimental model is verified by the simulation model. The accuracy of the developed simulation model with the experimental data are apparently very good (even more than 99% of the critical revolutions value obtained by calculation); however, it depends on the dynamic stiffness of the coupling. In this study, a detailed, comprehensive approach combining analytical procedures with simulation models is presented. Experimental data are verified with simulation results, which show a good agreement in the case of 700 kPa coupling pressure. The inaccuracy of some of the experiments (at 300 and 500 kPa pressures) is due to the interaction of the coupling's apparent stiffness and the level of the damped vibration energy in the coupling, which is manifested by its different heating. Based on further experiments, a solution to these problems will be proposed by introducing this phenomenon effectively into the simulation model.

Keywords: natural frequency; mode shape; piston machines; torsional vibration; pneumatic flexible coupling



Citation: Moravič, M.; Marasová, D.; Kaššay, P.; Ozdoba, M.; Lopot, F.; Bortnowski, P. Experimental Verification of a Compressor Drive Simulation Model to Minimize Dangerous Vibrations. *Appl. Sci.* **2024**, *14*, 10164. <https://doi.org/10.3390/app142210164>

Academic Editor: Mark J. Jackson

Received: 9 October 2024

Revised: 31 October 2024

Accepted: 2 November 2024

Published: 6 November 2024



Copyright: © 2024 by the authors. Licensee MDPI, Basel, Switzerland. This article is an open access article distributed under the terms and conditions of the Creative Commons Attribution (CC BY) license (<https://creativecommons.org/licenses/by/4.0/>).

1. Introduction

Nowadays, ever growing emphasis is being placed on low levels of vibration and noise generated during the operation of machinery and equipment and transmitted to the surrounding area. They represent a detrimental factor in terms of environmental and general operational safety [1]. Numerical simulation tools such as Fluent software and *k-ε* turbulence models are currently used to assess and control dangerous factors (including vibration) in the workplace [2].

Vibrations have a negative effect on the operation of mechanical systems and on the safety of operation—their reliability and also their service life are reduced [3–5]. It is generally known that various types of sources are involved in the generation of vibrations in the structural parts of the machine, mainly unbalance, misalignment, mechanical clearance of the bearings, resonance of the structure, bent shaft, excessive wear of bearings, damage to the gearing [6,7], lubrication [8–10], etc. These negative phenomena and their causes can be identified during the operation of the equipment by measuring the methods of technical diagnostics and monitoring [11–13]. As a result of inertial forces and variable load torque of individual machines and equipment, torsional oscillations occur [14–17]. Torsional vibration can be dangerous, depending on the level for a particular mechanical system and the place of its occurrence. In torsionally oscillating mechanical systems (mainly mechanical systems with internal combustion engines [18,19], piston compressors, piston pumps, and fans), which include flexible members, it is possible to reduce the dangerous torsional oscillation to an acceptable level by suitable adaptation of the dynamic properties (i.e., stiffness [20–24], damping coefficient [25], and mass moment of inertia [26]) of these members to the dynamics of the system [27,28]. However, this may not only apply to elastic members but also to other members in the mechanical system. Recent developments include so-called active vibration isolation, where an additional torque is generated in real time directly at the driving electric motor or a special active damper [29–32]. Dynamic properties largely affect the operation of the mechanical system, its lifetime, and reliability; therefore, to perform the above-mentioned procedure, the torsionally oscillating mechanical system needs to be appropriately tuned in advance [33]. The tuning of any mechanical system is most often verified on the basis of the results of the so-called Campbell diagram. It is used to determine whether resonance will occur [34]. The research of vibration problems in mechanical systems is not a new phenomenon in the field of engineering sciences. Vibrations represent phenomena occurring in every mechanical system since its manufacture. They are negative phenomena that interfere with the smooth operation of mechanical systems [35] and act as a threatening and risk factor. Therefore, it is both necessary and required to look for ways of their minimization [36,37].

Based on this fact, the main objective of this paper is to control the dangerous vibrations of the drive of a mechanical system by applying a pneumatic flexible coupling based on dynamic simulation models verified by experimental measurements. The main objective of the paper can be achieved by fulfilling the partial objectives, namely: selection of the comparison model, preparation of the mechanical system in the laboratory for experiments, obtaining input data for the model, calculation of natural frequencies and mode shapes, dynamic analysis, creation of the simulation model, realization of the experiments, verification of the model, and design of recommendations for control of dangerous vibrations.

2. Materials and Methods

With the development of new information and simulation technologies, sensors, and more and more methods are being used for the elimination of dangerous vibrations. Current approaches based on theoretical models using parameter-driven mathematical expressions to describe the mechanical system or monitoring-based data acquisition are no longer sufficient to ensure their reliability. Increasingly, these methods are being replaced by new techniques and software such as simulation models (e.g., digital twins) [38], or machine learning approaches [39]. Machine learning algorithms are difficult to interpret, and a large

volume and quality of data are required [40]. By integrating analytical models and online data with each other, digital twins will enable real-time control of mechanical systems.

2.1. Research Methodology

The design of the research methodology presented in this paper is based on the integration of analytical models and simulation models. To calculate the dynamic properties of aggregates, it is necessary to replace the aggregate with a suitable model of the mechanical system describing to some extent the real system before constructing the differential equations of motion. When calculating the dynamic phenomena of torsionally oscillating mechanical systems, the subject of the calculation is mainly the stress on the flexible couplings, as the weakest member of the mechanical system [41]. Here, it is appropriate to simplify the complex mechanical system as much as possible, but only enough to determine the stresses on the couplings with sufficient accuracy.

In order to achieve the research objective of controlling the dangerous vibration of the drive of the mechanical system by means of a flexible coupling based on simulation and experimental measurements, the following methodology was proposed (Figure 1).

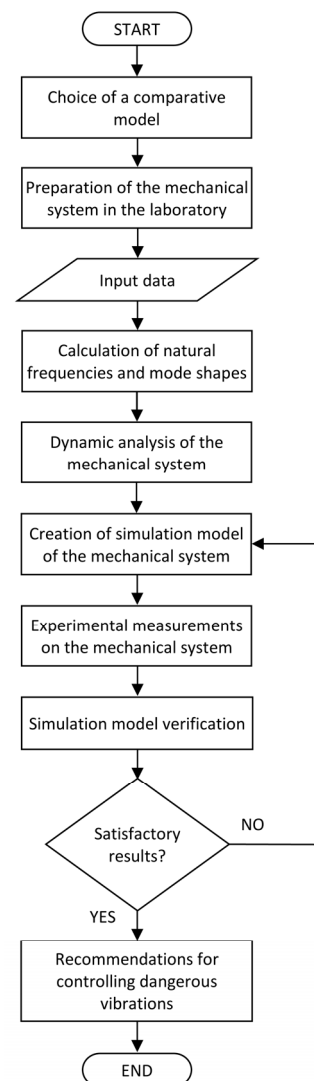


Figure 1. Research methodology.

In the reduction in masses in mechanical systems, the method of partial frequencies according to Rivin [42] was used. The mechanical system was reduced to a two-mass system. After calculating the natural frequency and the natural shape of the oscillation,

the Campbell diagram was processed to determine the critical revolutions. The dynamic calculation methodology of the mechanical system was applied in our research.

The dynamic analysis was carried out using a MATLAB program, which outputs the values of harmonic components of the torque transmitted by the flexible coupling. The output of the paper is the results of experimental verification of the simulation model of the mechanical system with variable torque operating at constant load and its comparison with the mathematical model.

2.2. Description of the Mechanical System

The subject of the research is a laboratory mechanical system driving a compressor by an electric motor (Figure 2). It is a mechanical system operating with variable torque at constant load. Between the rotating masses there is a pneumatic flexible coupling whose dynamic torsional stiffness can be varied during operation by changing the air pressure [27].

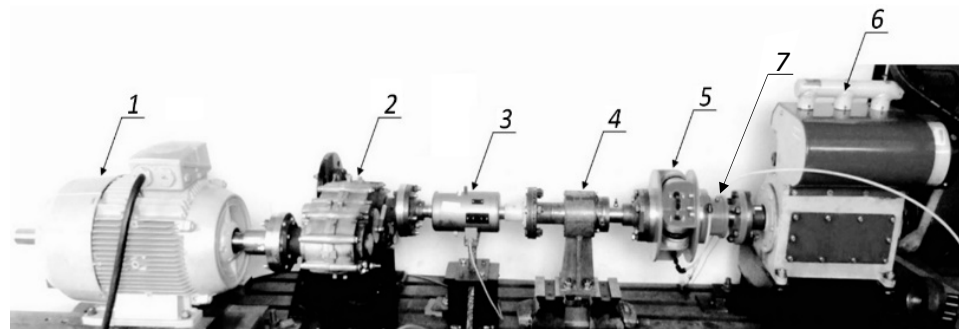


Figure 2. Experimental model of a mechanical system: 1—electric motor, 2—gearbox, 3—torque sensor, 4—bearing housing, 5—pneumatic flexible coupling, 6—three-cylinder piston compressor, 7—rotation supply.


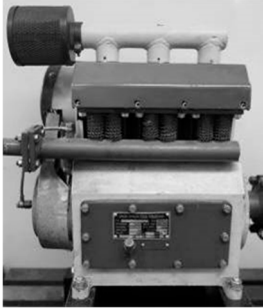


The revolutions of the electric motor (1) are continuously vector controlled by a frequency converter. The electric motor drives a three-cylinder ORLIK 3JSK-75 piston compressor (6) through a 1:1 gearbox (2) and a 4-1/70-T-C type pneumatic flexible coupling (5). The compressor is mounted on a rubber layer and has no flywheel; therefore, its impact on dynamics is higher. The compressed air from the compressor flows into an air pressure vessel with a capacity of 300 L. The compressed air is fed to the pneumatic coupling via a rotation supply (7). The magnitude of the torsional vibrations is measured by a torque sensor type 7934 MOM KALIBERGYAR (3). Table 1 describes the technical parameters of some members of the mechanical system.

The air pressure in the compression chamber of the pneumatic flexible coupling is measured by a pressure sensor. The signals from both sensors are amplified and processed by a universal eight-channel measuring device MX840 from the manufacturer HBM, and the data are subsequently sent to a PC (Figure 3) [43]. The operating revolutions of the mechanical system are $n_p = 600 \text{ min}^{-1}$.

Sensors used:

1. Torque sensor type 7934, manufacturer MOM KALIBERGYAR, measuring range 0–500 N·m, accuracy of the torque sensor is 0.1% of its measuring range, i.e., 0.5% (combined failure—nonlinearity, hysteresis, and reproducibility).
2. pressure sensor type MBS 3000, manufacturer Danfoss, overpressure measurement range 0–1 MPa, accuracy of the MBS 3000 sensor with metal diaphragm is 0.5% of its measurement range, i.e., 5 kPa (combined failure—non-linearity, hysteresis, and reproducibility).

Table 1. Basic parameters of some members of the mechanical system.

Elements of the Mechanical System	Parameters
Three-phase asynchronous motor 1LE1001-1DB234AF4-Z SIEMENS 	Nominal revolutions $n_N = 1470 \text{ min}^{-1}$ pri 50 Hz Mass moment of inertia $I_{AM} = 0.065 \text{ kg}\cdot\text{m}^2$ Synchronous revolutions $n_S = 1500 \text{ min}^{-1}$ Nominal power $P_N = 11 \text{ kW}$
Compressor 3JSK-75 ORLIK 	Mass moment of inertia $I_{PK} = 0.02967 \text{ kg}\cdot\text{m}^2$ Number of cylinders $i_{VPK} = 3$ Cylinder diameter $d_{VPK} = 82 \text{ mm}$ Piston stroke $z_{PPK} = 70 \text{ mm}$
Two-stage spur gearbox OBERAIGNER 	Gear ratio $i_p = 1:1$ Axial distance $a = 250 \text{ mm}$
Pneumatic flexible coupling 4-1/70-T-C 	Nominal torque $M_{KN} = 170 \text{ N}\cdot\text{m}$ Mass moment of inertia of the flange $I_{SA} = 0.06 \text{ kg}\cdot\text{m}^2$ Mass moment of inertia of the flange $I_{SB} = 0.07 \text{ kg}\cdot\text{m}^2$ Dynamic torsional stiffness: <ul style="list-style-type: none"> ■ $k_{DSMAX} = 2250 \text{ N}\cdot\text{m}\cdot\text{rad}^{-1}$ at pressure $p_S = 700 \text{ kPa}$ in the elastic element, ■ $k_{DSMAX} = 1780 \text{ N}\cdot\text{m}\cdot\text{rad}^{-1}$ at pressure $p_S = 500 \text{ kPa}$ in the elastic element, ■ $k_{DSMAX} = 1360 \text{ N}\cdot\text{m}\cdot\text{rad}^{-1}$ at pressure $p_S = 300 \text{ kPa}$ in the elastic element.

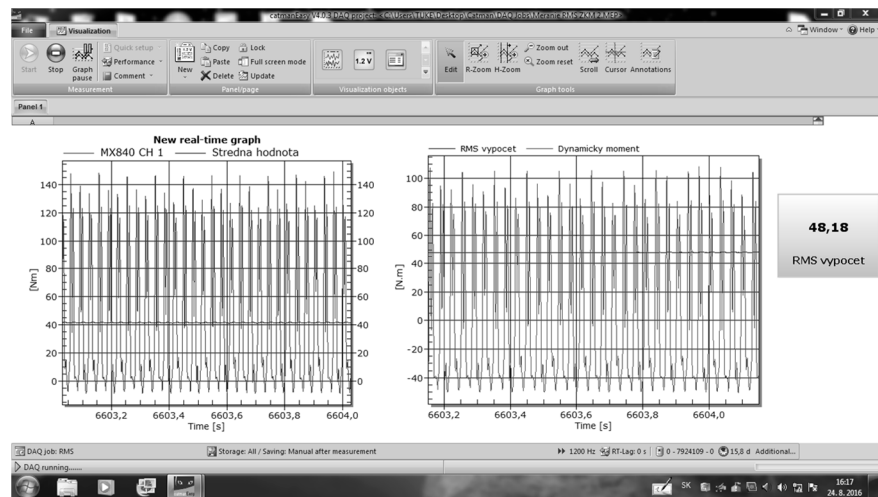


Figure 3. Time record from an experiment measurement in the CatmanEasy program.

3. Results and Discussion

3.1. Determination of the Operating State of the System in Terms of Resonance

The dynamic model (Figure 4) was created based on the known mechanical parameters of the compressor drive system. By means of the model, the values of natural frequencies and mode shapes were calculated as well as the Campbell diagram devised.

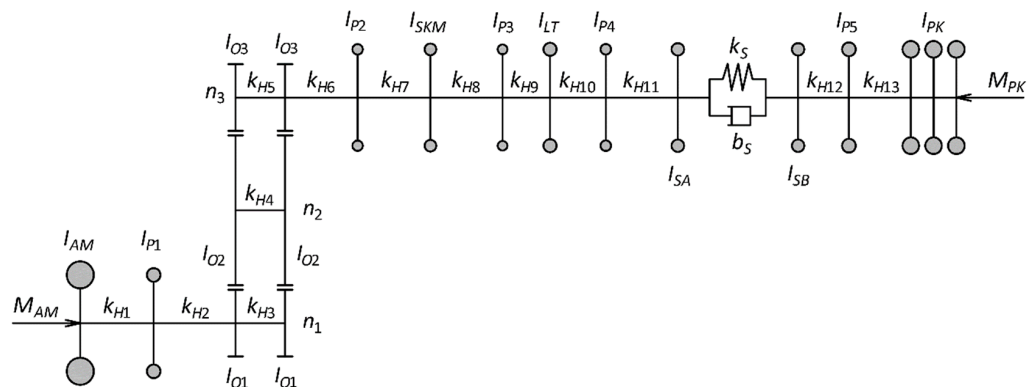


Figure 4. A complete replacement dynamic piston compressor drive model.

The individual elements for the dynamic model are listed in Table 2.

Table 2. Description of parameters of the system shown on Figure 4.

Parameter	Meaning
I_{AM}	Mass moment of inertia of the electric motor
I_{P1}	Mass moment of inertia of the flange behind the motor
I_{O1}, I_{O2}, I_{O3}	Mass moment of inertia of the gear
I_{P2}	Mass moment of inertia of the flange behind the gearbox
I_{SKM}	Mass moment of inertia of the torque sensor
I_{P3}	Mass moment of inertia of the flange behind the torque sensor
I_{LT}	Mass moment of inertia of the bearing housing
I_{P4}	Mass moment of inertia of the flange in front of the pneumatic coupling
I_{SA}	Mass moment of inertia of the flange of the pneumatic coupling
I_{SB}	Mass moment of inertia of the flange of the pneumatic coupling
I_{P5}	Mass moment of inertia of the flange behind the flexible coupling
I_{PK}	Mass moment of inertia of the piston compressor
$k_{H1}, k_{H2},$	Torsional stiffness of shafts between electric motor and gearbox

Table 2. Cont.

Parameter	Meaning
k_{H3}, k_{H4}, k_{H5}	Torsional stiffness of shafts in the gearbox
k_{H6}	Torsional stiffness of the shaft between I_{O3} and I_{P2}
k_{H7}	Torsional stiffness of the shaft between I_{P2} and I_{SKM}
k_{H8}	Torsional stiffness of the shaft between I_{SKM} and I_{P3}
k_{H9}	Torsional stiffness of the shaft between I_{P3} and I_{LT}
k_{H10}	Torsional stiffness of the shaft between I_{LT} and I_{P4}
k_{H11}	Torsional stiffness of the shaft between I_{P4} and I_{SA}
k_S	Torsional stiffness of the pneumatic coupling
k_{H12}	Torsional stiffness of the shaft between I_{SB} and I_{P5}
k_{H13}	Torsional stiffness of the shaft between I_{P5} and I_{PK}
b_S	Pneumatic coupling damping coefficient
M_{AM}	Electric motor torque
M_{PK}	Load torque of the piston compressor

The gear ratios between the shafts of the system are calculated as follows:

$$i_{1-2} = \frac{n_1}{n_2}, i_{2-3} = \frac{n_2}{n_3}, i_{1-3} = \frac{n_1}{n_3}. \tag{1}$$

Assuming that the shaft stiffnesses $k_{H3}, k_{H4},$ and k_{H5} (Figure 4) show a higher value than the other stiffnesses and the input shaft revolutions of the gearbox are equal to the output shaft revolutions $n_1 = n_3$, a reduction as shown in Table 3 could be done. This reduction is applied to the high-revolution shaft with stiffness k_{H1} .

Table 3. Reduction in mass moments of inertia and torsional stiffness on the high-revolution shaft.

Mass Moments of Inertia		Element Torsional Stiffnesses	
$I_1 = I_{AM}$	$I_7 = \frac{I_{LT}}{i_{1-3}^2}$	$k_1 = k_{H1}$	$k_7 = \frac{k_{H10}}{i_{1-3}^2}$
$I_2 = I_{P1}$	$I_8 = \frac{I_{P4}}{i_{1-3}^2}$	$k_2 = k_{H2}$	$k_8 = \frac{k_{H11}}{i_{1-3}^2}$
$I_3 = 2 \cdot I_{O1} + \frac{2 \cdot I_{O2}}{i_{1-2}^2} + \frac{2 \cdot I_{O3}}{i_{1-3}^2}$	$I_9 = \frac{I_{SA}}{i_{1-3}^2}$	$k_3 = \frac{k_{H6}}{i_{1-3}^2}$	$k_9 = \frac{k_S}{i_{1-3}^2}$
$I_4 = \frac{I_{P2}}{i_{1-3}^2}$	$I_{10} = \frac{I_{SB}}{i_{1-3}^2}$	$k_4 = \frac{k_{H7}}{i_{1-3}^2}$	$k_{10} = \frac{k_{H12}}{i_{1-3}^2}$
$I_5 = \frac{I_{SKM}}{i_{1-3}^2}$	$I_{11} = \frac{I_{P5}}{i_{1-3}^2}$	$k_5 = \frac{k_{H8}}{i_{1-3}^2}$	$k_{11} = \frac{k_{H13}}{i_{1-3}^2}$
$I_6 = \frac{I_{P3}}{i_{1-3}^2}$	$I_{12} = \frac{I_{PK}}{i_{1-3}^2}$	$k_6 = \frac{k_{H9}}{i_{1-3}^2}$	—

A dynamic model with twelve-mass discs after the first reduction is shown in Figure 5.

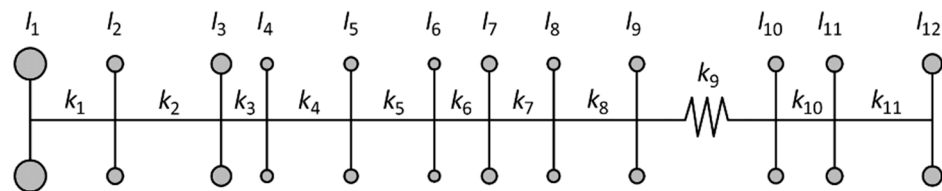


Figure 5. A twelve-mass chain mechanical system.

Using the method of partial frequencies [42], this twelve-mass system was reduced to a two-mass system. The resulting values after reduction by this method usually show an accuracy of 3–5% [42,44].

The dynamical model of this reduced two-mass mechanical system is shown in Figure 6.

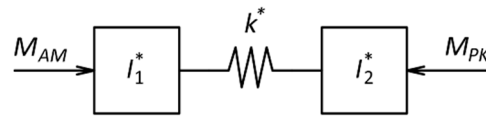


Figure 6. Two-mass reduced mechanical system.

The analysis of torsional vibration of a mechanical system is based on a system of differential equations of motion. The equations describing a two-mass reduced mechanical system without damping (Figure 6) have the following form:

$$I_1^* \cdot \ddot{\varphi}_1 + k^* \cdot (\varphi_1 - \varphi_2) = M_{AM}, \tag{2}$$

$$-I_2^* \cdot \ddot{\varphi}_2 + k^* \cdot (\varphi_1 - \varphi_2) = M_{PK}. \tag{3}$$

The variable load torque of a piston compressor is given by:

$$M_{PK} = M_{NPK} + \sum_{i=1}^{\infty} M_{iPK} \cdot \cos(i \cdot \omega_{PK} \cdot t + \gamma_{iPK}). \tag{4}$$

The mode shape of the oscillation at coupling pressure is shown in Figure 7.

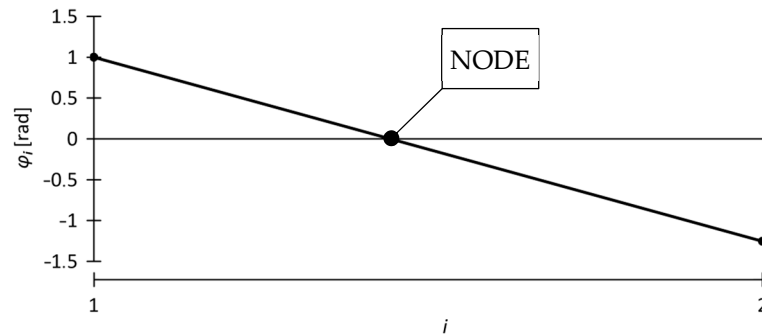


Figure 7. Mode shape of the strain curve for $\Omega_0 = 201.431 \text{ rad} \cdot \text{s}^{-1}$.

A Campbell diagram is an interference diagram that identifies possible matches between the expected excitation frequencies and the calculated natural torsional frequencies over the operating speed range. Each ascending line on the interference diagram represents a single mechanical or electrical excitation frequency or harmonic; when they intersect with the torsional natural frequency (horizontal line), torsional resonance occurs. The intersection of those lines indicates a possible torsional resonance condition. For some systems, an interference diagram may be all that is needed to show that torsional resonances will not be excited [45,46].

Figure 8 shows the Campbell diagram for a system operating at coupling pressure 700 kPa with the following parameters marked in it: the operating rotational frequency $n_p = 600 \text{ min}^{-1}$, the critical revolutions from the principal harmonic element $n_{K3} = 641.2 \text{ min}^{-1}$ and the natural rotational frequency $N_0 = 1923.526 \text{ min}^{-1}$.

The detuning coefficient for the i -th harmonic component is defined by the formula:

$$\eta_i = \frac{n \cdot i}{N_0}. \tag{5}$$

Table 4 gives the detuning coefficients of the harmonic components operating rotational frequency $n_p = 600 \text{ min}^{-1}$. Since this is a three-cylinder piston compressor, the main harmonic components will be integer multiples of the third harmonic component.

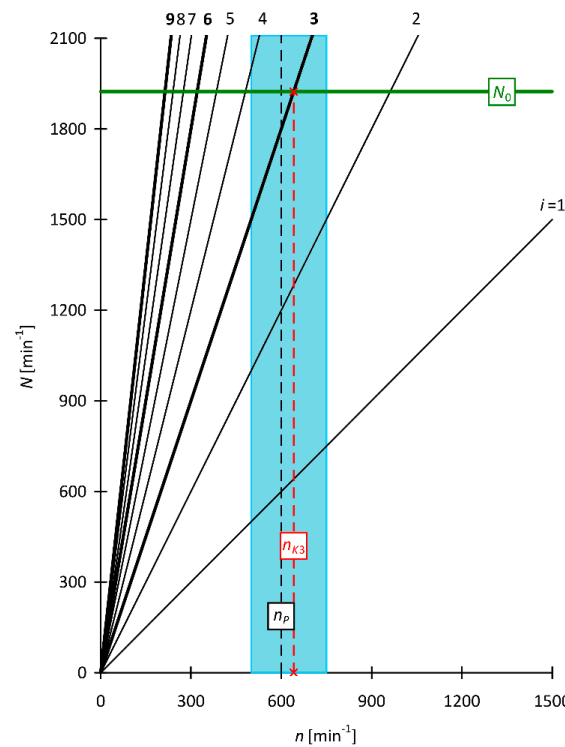


Figure 8. Campbell diagram of the mechanical system studied.

Table 4. The detuning coefficient of the selected harmonic components at coupling pressure 700 kPa.

i	1	2	3	4	5	6
η_i	0.312	0.624	0.936	1.248	1.560	1.872

These will always appear during the load torque; the other harmonic components are the so-called secondary harmonic components, which will only appear if the compressor cylinders do not operate evenly [45–48].

According to the literature [27], the system operates in the resonance region if:

$$0.8 < \eta_i < 1.2. \tag{6}$$

From the results shown in Table 4, we can say that the system at coupling pressure 700 kPa operates in the resonance region.

3.2. Dynamic Calculation of a Mechanical System Under Forced Oscillation

To calculate the excitation of the forced oscillation, we based it on the aforementioned compressor parameters, where we first determined the p - V diagram of the operating cycle of a single cylinder of a three-cylinder piston compressor, which is contained in Figure 9.

Figure 10 is already a graphical representation of the total load torque M_C and its mean load torque M_S at the crankshaft from all three cylinders of the compressor.

In this case, it is a fault-free condition of the piston compressor. The amplitudes and phases of the harmonic components of the dynamic torque in the fault-free condition are described in Table 5.

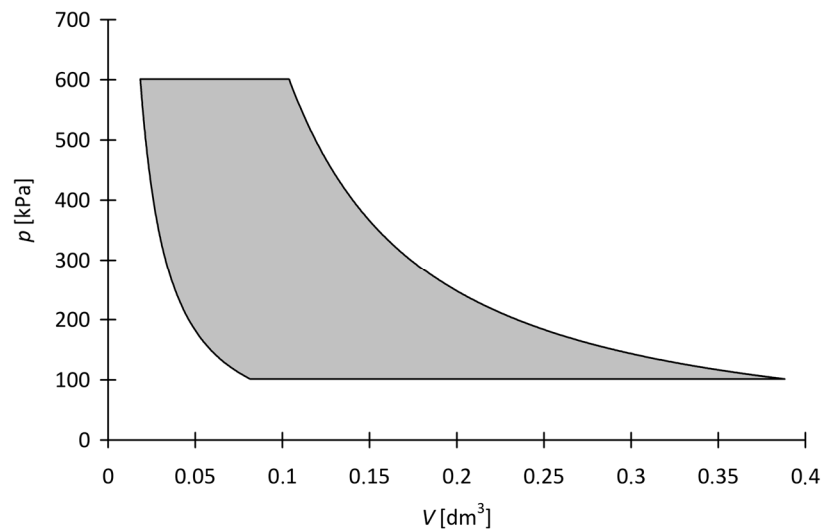


Figure 9. p - V diagram of piston compressor cylinder.

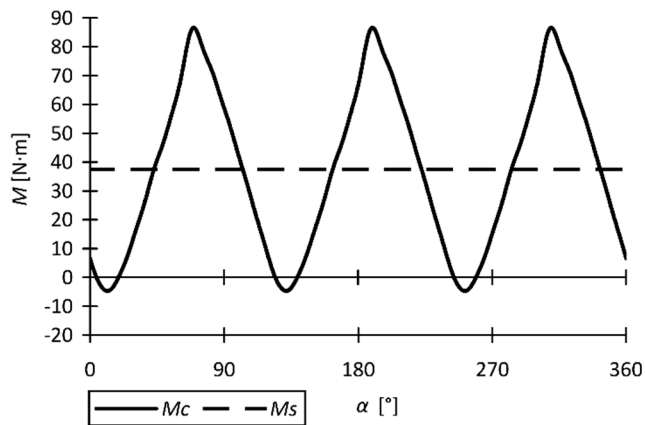


Figure 10. The total load torque M_C vs. the rotation angle of the crankshaft of the piston compressor and its static component M_S .

Table 5. Amplitudes and phases of harmonic components of the dynamic torque of the piston compressor.

i	M_{iPK} [N·m]	γ_{iPK} [rad]	i	M_{iPK} [N·m]	γ_{iPK} [rad]
1	0	0	7	0	0
2	0	0	8	0	0
3	40.381	3.804	9	3.658	4.818
4	0	0	10	0	0
5	0	0	11	0	0
6	1.394	1.286	12	1.233	1.976

3.3. Dynamic Calculation of the Mechanical System at Steady Compressor Operation

Figure 11 plots the calculated time waveform of the dynamic torque transmitted by the coupling for the duration of one operating cycle (one crankshaft revolution) of a piston compressor at its steady-state operation and operating revolutions $n_p = 600 \text{ min}^{-1}$.

The hysteresis loop of the pneumatic flexible coupling (Figure 12) was plotted from the time waveform (Figure 11).

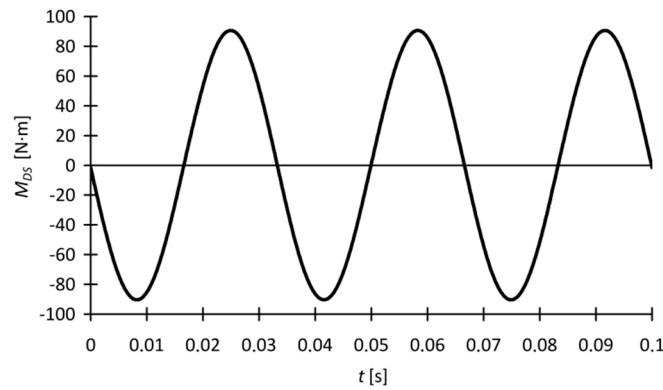


Figure 11. Development over time of dynamic torque transmitted by a pneumatic flexible coupling at pressure 700 kPa.

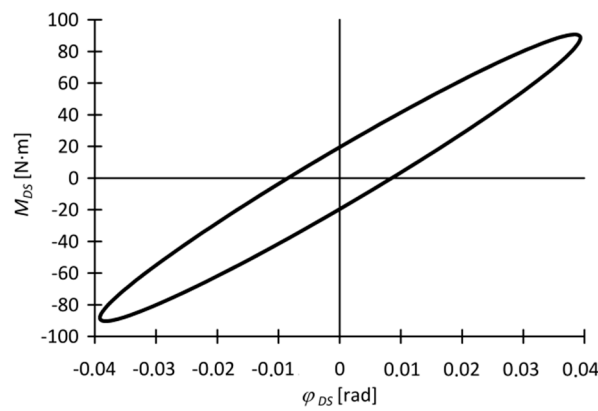


Figure 12. Hysteresis loop of flexible pneumatic coupling at pressure 700 kPa.

The amplitude of the dynamic load torque transmitted by the pneumatic coupling as a function of revolutions is shown in Figure 13.

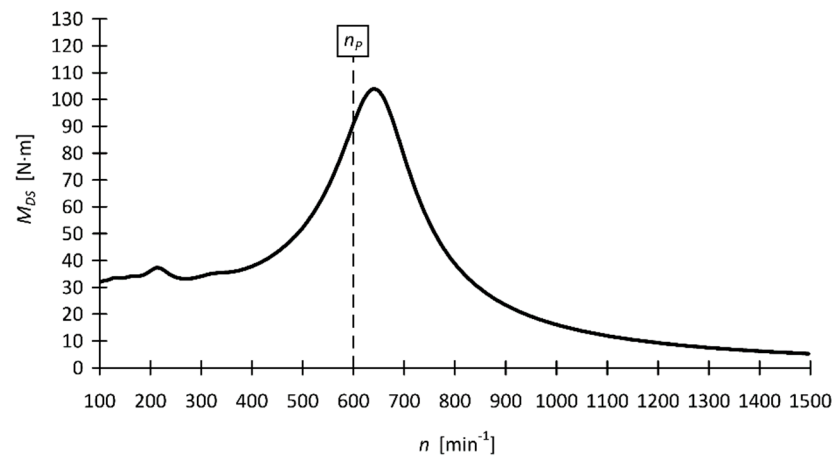


Figure 13. Dynamic load torque transmitted by the flexible pneumatic coupling at pressure 700 kPa.

In order to compare the result of the effective value of the dynamic load torque component of the $RMS M_{DS}$ simulation model with the experimental model, we modified the M_{DS} (Figure 13) to the $RMS M_{DS}$ (Figure 14).

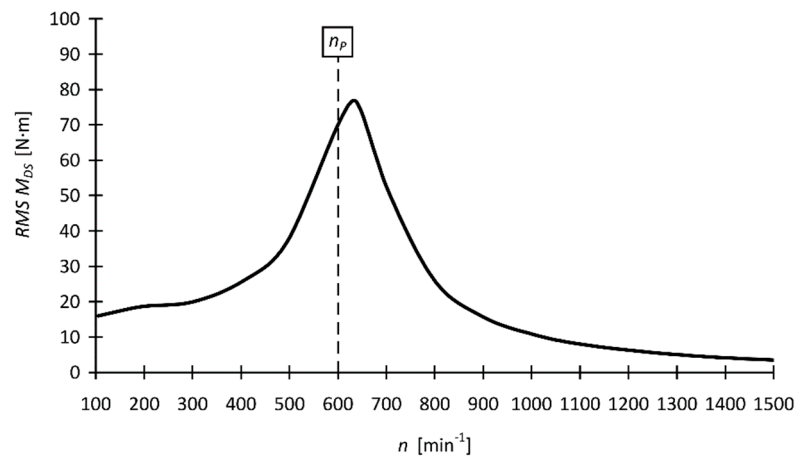


Figure 14. The effective value of the dynamic component of the torque $RMS M_D$ transmitted by the pneumatic flexible coupling at pressure 700 kPa.

3.4. Simulation Model for Steady (Even) Compressor Operation

In technical practice, as already mentioned, machine failures often occur, such as cylinders falling out of action. The following section is devoted to this issue. The failure of one cylinder was simulated by setting its overpressure value at displacement against atmospheric pressure to $p = 0$ Pa. Figure 15 shows the calculated waveform of the total load torque M_C and mean load torque M_S at the compressor crankshaft.

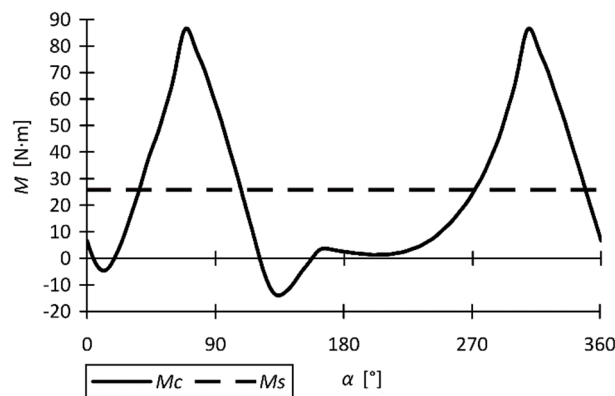


Figure 15. Total load torque M_C depending on the angle of rotation of the α crankshaft when the cylinder of the piston compressor is out of operation and its static component M_S .

Table 6 gives the amplitudes and phases of the harmonic components of the load torque with one cylinder out of operation.

Table 6. Amplitudes and phases of harmonic components of the dynamic torque of the piston compressor with one cylinder out of operation.

i	M_{iPK} [N·m]	γ_{iPK} [rad]	i	M_{iPK} [N·m]	γ_{iPK} [rad]
1	22.804	0.039	7	1.507	0.61
2	19.55	3.4	8	1.676	4.321
3	26.664	3.786	9	2.438	4.817
4	7.84	4.43	10	0.739	5.056
5	3.163	1.884	11	0.526	1.917
6	0.917	1.33	12	0.826	1.989

Figure 16 shows the time waveform of the dynamic load torque transmitted by the pneumatic flexible coupling with one cylinder out of operation.

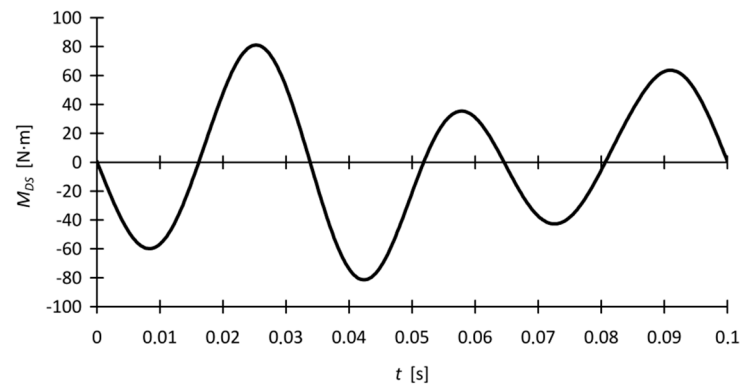


Figure 16. Development over time of the dynamic torque M_{DS} transmitted by a pneumatic flexible coupling at pressure 700 kPa with the cylinder out of operation.

The hysteresis loop of the pneumatic flexible coupling in Figure 17 was derived from Figure 16.

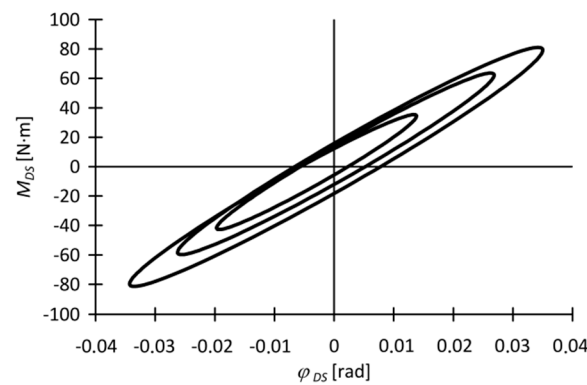


Figure 17. Pneumatic flexible coupling hysteresis loop at pressure 700 kPa with the cylinder out of operation.

Figure 18 describes the waveform of the amplitude of the dynamic load torque transmitted by the pneumatic flexible coupling with one cylinder out of operation as a function of revolutions.

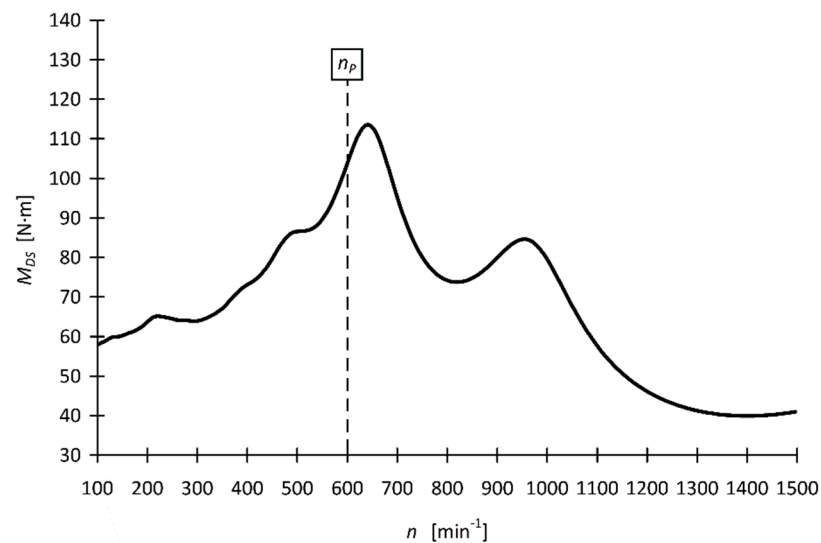


Figure 18. Dynamic torque M_{DS} transmitted by pneumatic flexible coupling at pressure 700 kPa with the cylinder is out of operation.

Figure 19 shows the effective value of the dynamic component of the load torque M_{DS} to compare with the experiment.

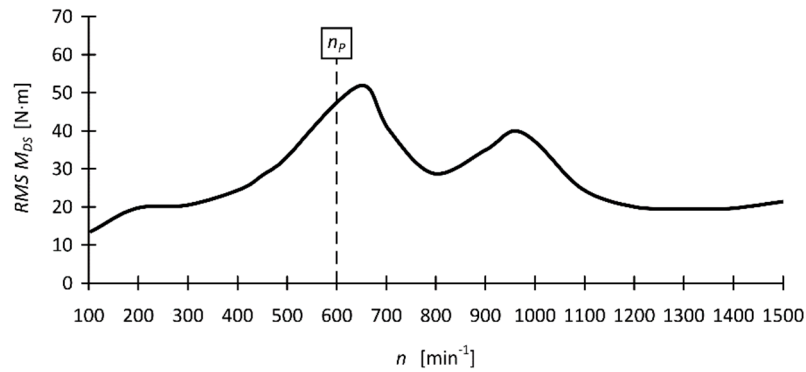


Figure 19. Effective value of the dynamic component of the load torque M_{DS} transmitted by a pneumatic flexible coupling at pressure 700 kPa with the cylinder out of operation.

For additional pressures in the elastic element of the coupling, the resulting waveforms are given in Tables 7 and 8.

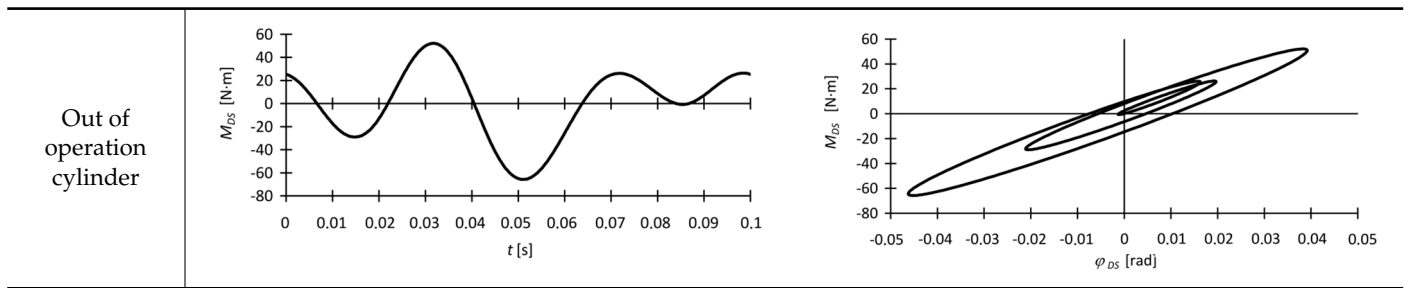
Table 7. Dynamic torque-time waveform M_{DS} and hysteresis loop at pressure $p_S = 500$ kPa in the elastic element.

		$k_{DS} = 1780 \text{ N}\cdot\text{m}\cdot\text{rad}^{-1}$	
Steady state			

Table 8. Dynamic torque-time waveform M_{DS} and hysteresis loop at pressure $p_S = 300$ kPa in the elastic element.

		$k_{DS} = 1360 \text{ N}\cdot\text{m}\cdot\text{rad}^{-1}$	
Steady state			

Table 8. Cont.



3.5. Simulation of the Output Signals on the Coupling Using Fourier Transformation

For the frequency analysis, a MATLAB simulation program was used to input the amplitudes and phases of the harmonic components of the dynamic torque. The given program also offers the possibility to choose filters (Hamming window and Hann window). The flow and results of the MATLAB analysis for the dynamic torque on the flexible coupling are shown in Figures 20 and 21.

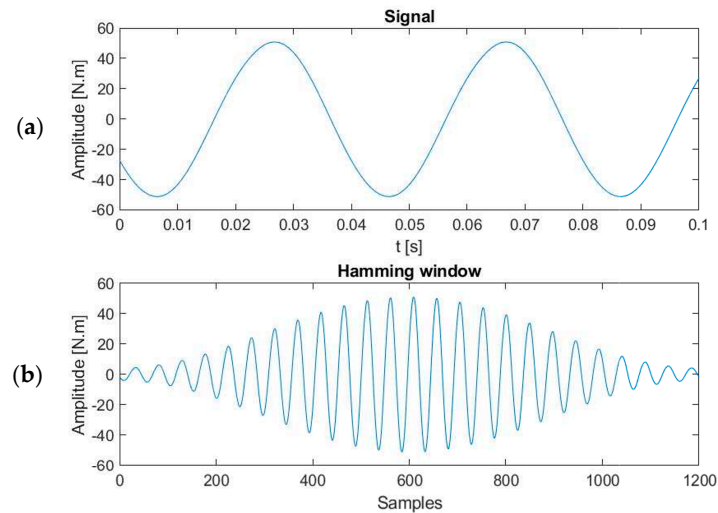


Figure 20. Signal (a) and Hamming window (b) at coupling pressure $p_S = 700$ kPa and revolutions $n = 500 \text{ min}^{-1}$.

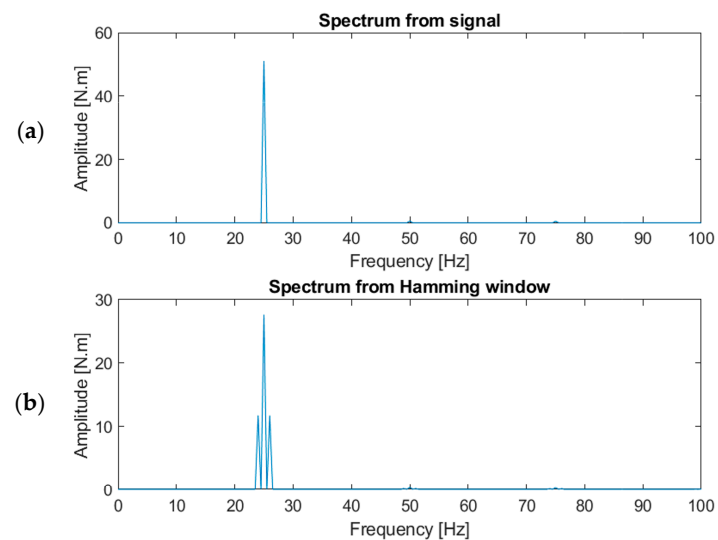


Figure 21. Spectrum from the signal (a) and Hamming window (b).

3.6. Verification of the Simulation Model Using Experimental Measurement

After the description of the mechanical system of the compressor drive and the dynamic calculations performed, a description of the experimental measurement follows to determine the torsional vibration values in the mechanical system consisting of a three-cylinder air compressor, driven by an electric motor using a pneumatic flexible coupling.

Measuring the Course of the Resonance Curve

The measurement was carried out with steady (even) cylinder operation and then using a rejector so that one cylinder could be disabled by opening the compressor suction valve. The calculation of the effective value of the dynamic component of the load torque $RMS M_D$, which is transmitted by the coupling, was the starting point for determining the magnitude of torsional vibration. The formula for its calculation was

$$RMS M_D = \sqrt{\frac{1}{N} \cdot \sum_{i=1}^N (M_{Di})^2}, \quad (7)$$

where

$$M_{Di} = M_i - \left(\frac{1}{N} \cdot \sum_{i=1}^N M_i \right), \quad (8)$$

where M_i is the i -th signal sample.

The above result from this formula indicates that it was necessary to measure the time course over time of the total load torque, from which the dynamic component M_D was filtered out. In the next calculation of $RMS M_D$, a moving average was used. The values were read after a steady state was reached. The measurement was carried out at varying revolutions in the range from $n = 105 \text{ min}^{-1}$ to $n = 1500 \text{ min}^{-1}$, at a pressure in the compression chamber of the pneumatic flexible coupling $p_S = 700 \text{ kPa}$, $p_S = 500 \text{ kPa}$ and $p_S = 300 \text{ kPa}$. The compressor output pressure is set to a constant value, $p_N = 500 \text{ kPa}$. The time signal (Figure 3) load torque was recorded with a sampling rate of $f_V = 1200 \text{ Hz}$ (number of samples $N = 2400$) with steady (even) cylinder operation and then with one compressor cylinder out of operation.

The Campbell diagram (Figure 22) for pressure coupling 700 kPa compiled from the measured values also contains marked, predetermined operating revolutions and critical revolutions from the principal harmonic. Based on the point of intersection of the critical revolutions and the beam (harmonic component) on the diagram, it is possible to determine the value of the rotational natural frequency N_0 and calculate the natural frequency f_0 and the angular natural frequency Ω_0 . From what is shown, it follows that resonances at higher values of $RMS M_D$ occur at compressor revolutions of approximately $n_{K3} = 638 \text{ min}^{-1}$. These are resonances from the main harmonic component of the torque of the three-cylinder compressor $i = 3$. When the cylinder is out of operation, resonances occur from both the main and the secondary components at critical $n_{K4} = 450 \text{ min}^{-1}$, $n_{K3} = 660 \text{ min}^{-1}$ and $n_{K2} = 956 \text{ min}^{-1}$.

From the measured values, the development of the static (central) load torque is plotted (Figure 23).

Figure 24 shows the resonance curve, i.e., the $RMS M_D$ waveform depending on the revolutions n of the mechanical system.

When the cylinder was out of operation (Figure 25), the value of the effective value of the dynamic component of the load torque $RMS M_D$ decreased as compared to Figure 24, but secondary harmonic components were manifested.

Shown below is the development of frequency analysis at revolutions $n = 500 \text{ min}^{-1}$ (Figures 26 and 27). The first representation describes the use of the Hamming window when running evenly, and the second after one cylinder was out of operation.

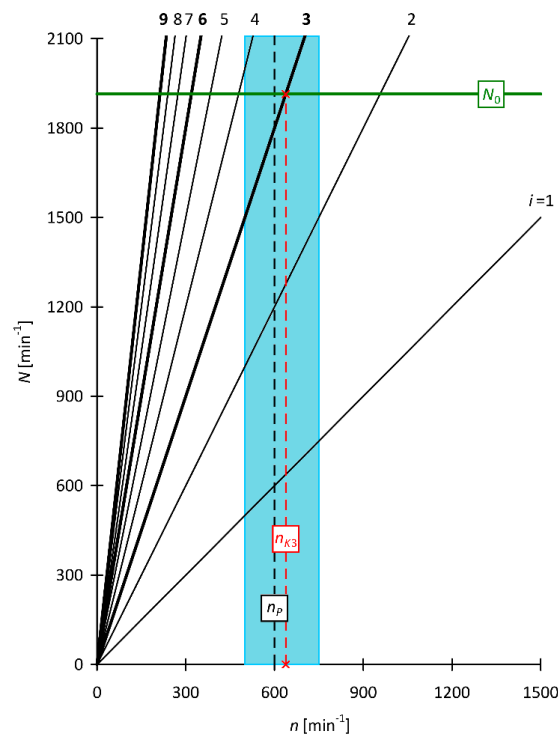


Figure 22. Campbell diagram of the mechanical system from the measured values.

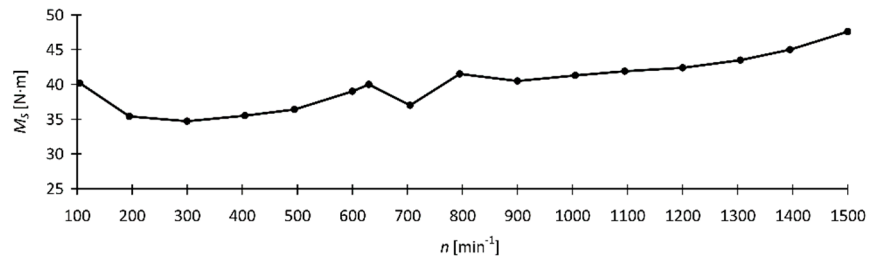


Figure 23. Development of the static component of load torque M_S depending on the engine revolutions n at pressure 700 kPa.

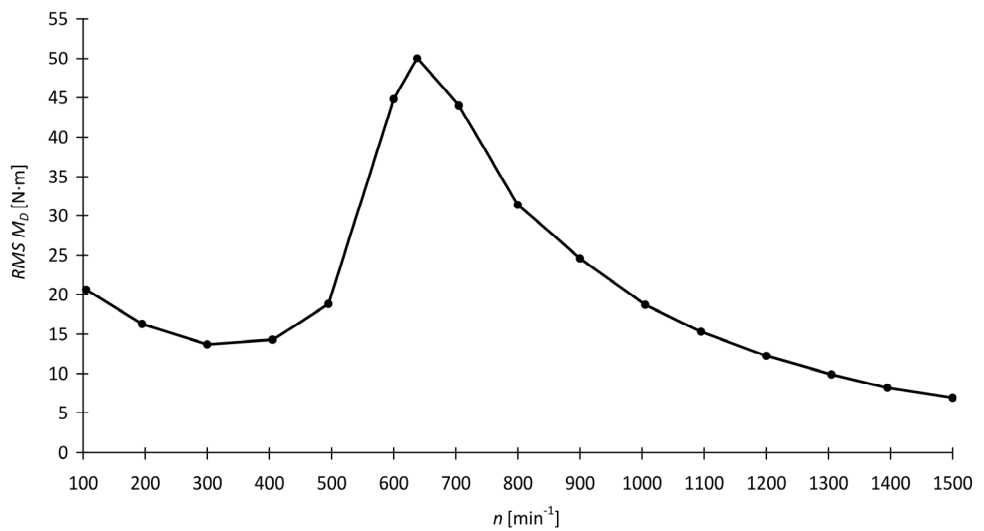


Figure 24. Effective value of the dynamic component of the load torque $RMS M_D$ of the pneumatic flexible coupling at pressure 700 kPa vs. the engine revolutions n – steady state.

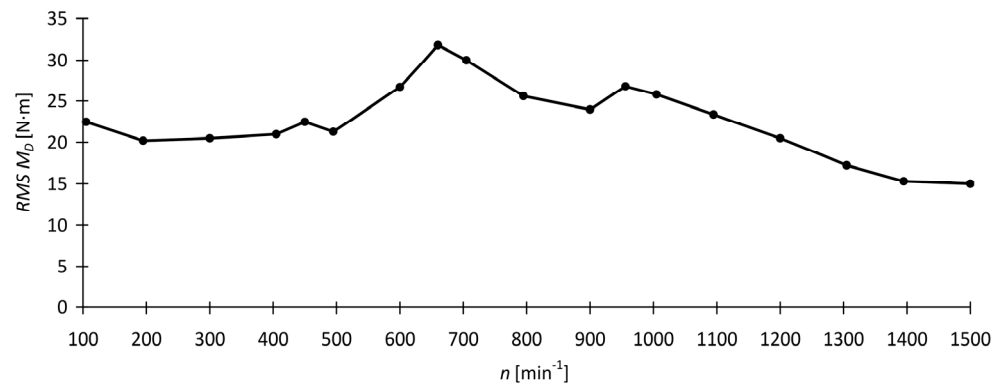


Figure 25. Effective value of the dynamic component of the load torque $RMS M_D$ of the pneumatic flexible coupling at pressure 700 kPa vs. the engine revolutions n with the cylinder out of operation.

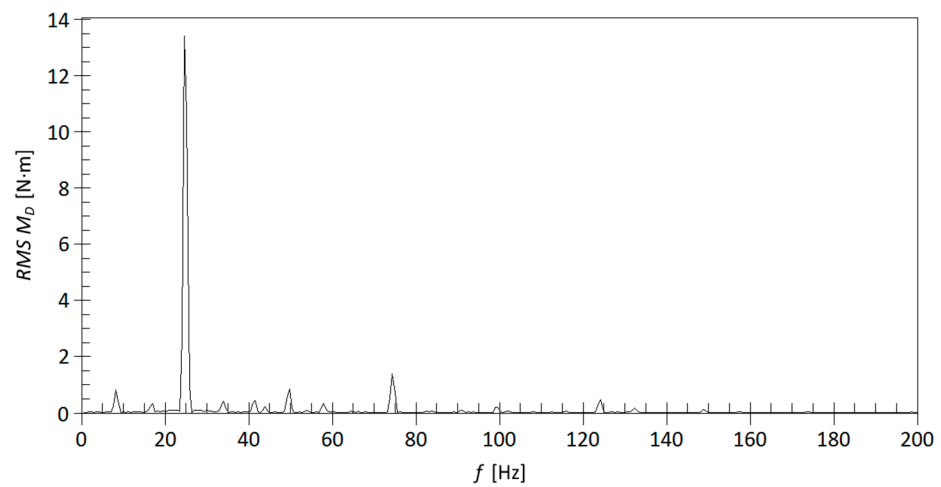


Figure 26. Frequency analysis using a Hamming window at $n = 500 \text{ min}^{-1}$ at steady operation.

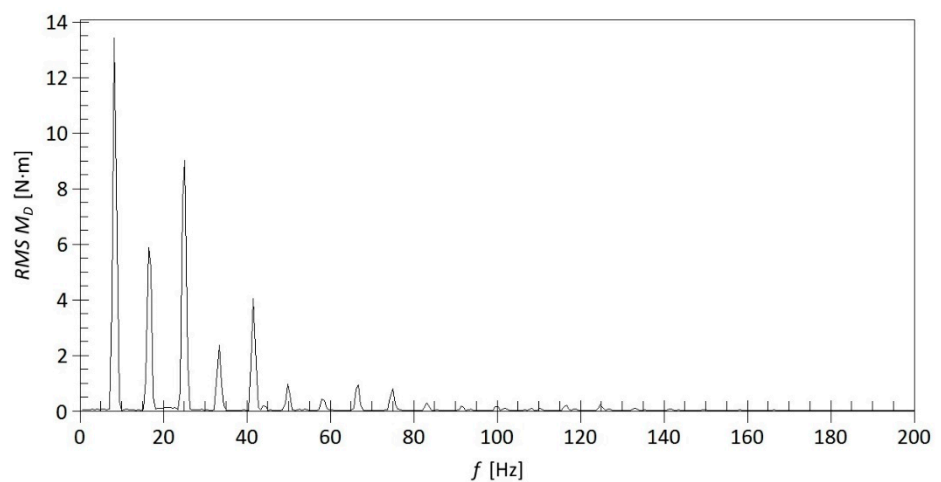


Figure 27. Frequency analysis using a Hamming window at $n = 500 \text{ min}^{-1}$ and one cylinder out of operation.

4. Comparison of Experimental and Simulation Models

The comparison of the experimental model in the laboratory with the simulation model was mainly aimed at determining the position of the critical revolutions based on the waveform of the effective value of the dynamic component of the $RMS M_D$ load torque. The comparison of the experimental and simulation model results is shown in Figures 28–33, where the waveforms of the effective values of the dynamic component

of the load torque $RMS M_D$ as a function of the steady-state and dropped single cylinder revolutions at pressures of 700, 500, and 300 kPa, respectively, are compared.

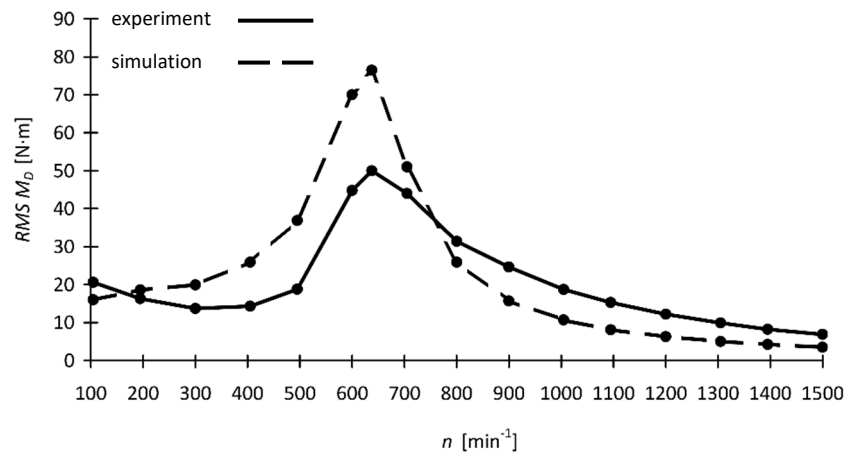


Figure 28. Comparison of the characteristics at steady operation of a piston compressor—pressure in the elastic element of the coupling $p_S = 700$ kPa.

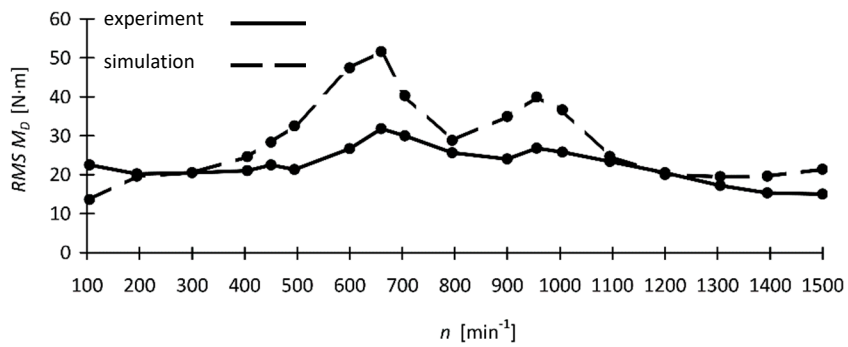


Figure 29. Comparison of the characteristics at one cylinder out of operation of a piston compressor—pressure in the elastic element of the coupling $p_S = 700$ kPa.

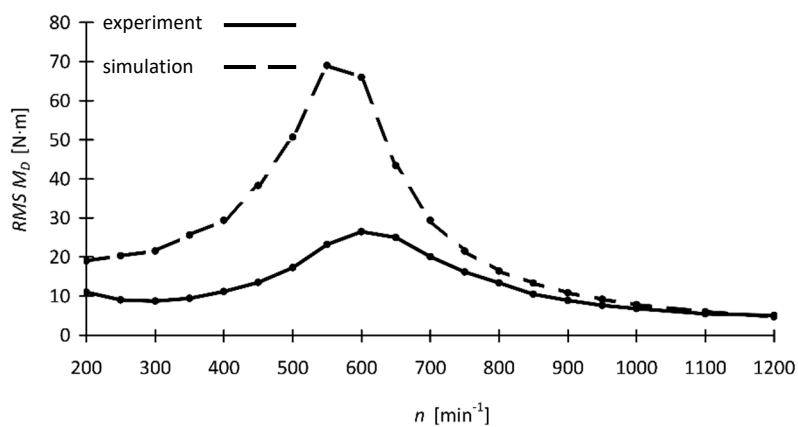


Figure 30. Comparison of the characteristics at steady operation of a piston compressor—pressure in the elastic element of the coupling $p_S = 500$ kPa.

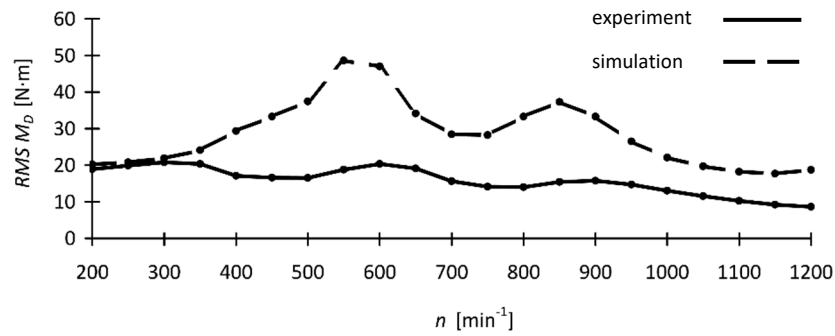


Figure 31. Comparison of the characteristics at one cylinder out of operation of a piston compressor—pressure in the elastic element of the coupling $p_S = 500$ kPa.

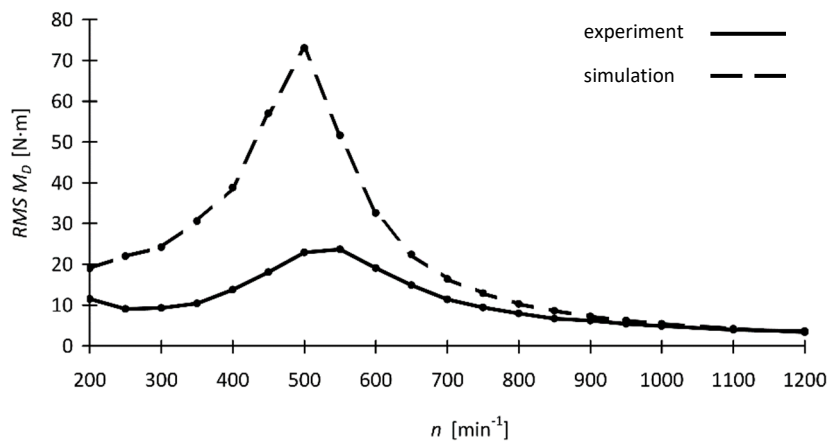


Figure 32. Comparison of the characteristics at steady operation of a piston compressor—pressure in the elastic element of the coupling $p_S = 300$ kPa.

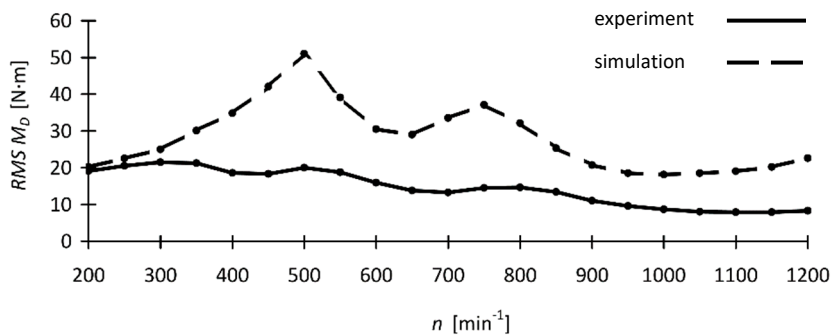


Figure 33. Comparison of the characteristics at one cylinder out of operation of a piston compressor—pressure in the elastic element of the coupling $p_S = 300$ kPa.

Table 9 shows the values of the natural circular frequencies obtained from the solution of the simulation model and the realization of the experimental measurements for the steady-state operation at pressure $p_S = 700$ kPa, $p_S = 500$ kPa, and $p_S = 300$ kPa in the elastic element of the coupling.

Accuracy in terms of the meaning of correspondence between the calculated and experimentally determined critical revolutions is determined as the ratio of experimentally determined revolutions to the revolutions determined by calculation. The sign (+) in the column indicates an increase, and the sign (−) indicates a decrease in the value of the critical revolutions determined experimentally compared to the value of the critical revolutions determined by calculation.

Table 9. Comparison of simulation and experimental results.

Pressure in Coupling [kPa]	Parameter	Value [rad·s ⁻¹]	Parameter	Value [min ⁻¹]	Accuracy [%]
700	Ω_{0SIM}	201.431	n_{K3SIM}	641	−0.47
	Ω_{0EXP}	200.434	n_{K3EXP}	638	
500	Ω_{0SIM}	179.167	n_{K3SIM}	570	5.26
	Ω_{0EXP}	188.496	n_{K3EXP}	600	
300	Ω_{0SIM}	156.610	n_{K3SIM}	498	10.44
	Ω_{0EXP}	172.788	n_{K3EXP}	550	

In general, the difference between the results can be caused by a number of different factors and their combination:

- Incomplete information on the input parameters, i.e., torsional shaft stiffness and mass moments of inertia.
- The method used to determine the natural frequencies and mode shapes of oscillations;
- Tooth clearance in the gearbox.
- The effect of frequency on the stiffness of the flexible coupling.
- Influence of the value of the mean torque and amplitude on the equivalent torsional stiffness of the flexible coupling (non-linearity of the loading characteristic of the coupling);
- Torsional vibration in the gearbox.
- Tongues clearance in individual flanges.
- Ambient temperature not included in the calculation.
- Temperature of elastic elements not included in the simulation model.
- Location of the torque meter.
- Insufficient heat dissipation from the piston compressor in operating mode.
- Maintaining and regulating constant pressure by a throttle valve at the outlet of the pressure tank.
- Operating revolutions close to the resonance from the main harmonic component in steady (even) operation.

Because the decrease in accuracy presented in Table 9 corresponds very well with the decrease in coupling stiffness due to temperature, it can be stated that the main cause of the decreasing agreement of the results is precisely this phenomenon. As can be seen, the results differ from each other in the order of units of percent. It can also be stated that the lower stiffness of the connection leads to higher torsional deflections of the oscillating masses, which are manifested by its intense heating. It is therefore very important to capture this aspect and include it in computational models.

5. Conclusions

The main focus of the research was vibrations, or torsional oscillations, often accompanying the operation of mechanical systems. These disturbances, if not controlled, result in machine unreliability in mechanical systems, compromising the safe operation of the plant. Based on the general knowledge of vibration and the known parameters of a real laboratory mechanical system, a simulation model was developed. The original twelve-mass mechanical system was reduced to a two-mass system by the partial frequency method. The MATLAB simulation program was used in the calculations and analyses.

The results obtained by calculation were experimentally verified by measurements on a laboratory mechanical system. After comparing the calculated natural angular frequency with the measured value, we can evaluate that the applied mathematical model is accurate to 99.53% at 700 kPa coupling pressure.

In potential future research, it is possible to include the temperature value of the elastic element of the coupling in the calculations and to determine more accurately the mass moments of inertia of the individual members of the mechanical system.

At the same time, it is planned to include in the simulation the occurrence of non-equilibrium condensation in the compressor, taking into account the research results presented in publications [49–51].

The aim of our paper is to show the importance of analytical calculations in estimating the natural frequencies and the corresponding mode shapes of oscillations in engineering work.

A mathematical model for a torsionally oscillating mechanical system has been developed where the stiffness of the elastic coupling can be continuously varied. Thus, the critical revolutions at different stiffnesses (pressures in the coupling) can be determined.

It was solved in steady state with harmonic excitation, amplitude, and phase over resonance curves for the individual harmonic components, which were then summed. We have simplified the multi-mass system to a two-mass system to analyze the effect of oscillations on the elastic coupling. This is under the condition of accuracy, where the frequencies differed from each other minimally.

Benefits of the simulation model:

- The mass reduction method used allows the use of a two-mass instead of a multi-mass system, which greatly simplifies the calculations.
- We can calculate the critical revolutions as a function of coupling pressure quite accurately. So, with a system operating with a range of operating revolutions, we can avoid resonance without having to directly measure the torque; we just need to know the revolutions, and we can determine the appropriate pressure accordingly.
- Characteristic depending on the ratio of the critical revolutions to the coupling pressures.

Author Contributions: Conceptualization, M.M., P.K. and F.L.; methodology, M.M. and D.M.; software, M.M.; validation, P.K. and F.L.; formal analysis, D.M. and M.M.; investigation, M.M. and P.K.; resources, M.M. and P.K.; data curation, M.M.; writing—original draft preparation, M.M.; writing—review and editing, P.B. and M.O.; visualization, M.M., P.B. and M.O.; supervision, P.K.; project administration, D.M.; funding acquisition, D.M. All authors have read and agreed to the published version of the manuscript.

Funding: This research was funded by the Slovak Research and Development Agency under contract No. APVV-23-0342 “New structural and material elements for sustainable transport of bulk materials” and APVV SK-PL-23-0052 “Modeling of transverse vibrations of belt and diagnostics of pipe conveyors” and from the project KEGA 037TUKE-4/2024 “Creation of interactive tool for increasing of students’ skills and competences in teaching of study subjects relating to elaboration of drawing documentation” and VEGA 1/0728/24 “Research on the possibilities of implementing sensory technologies and visualization methods for the needs of digital transformation of pipeline conveyor systems”.

Institutional Review Board Statement: Not applicable.

Informed Consent Statement: Not applicable.

Data Availability Statement: Data are contained within the article.

Conflicts of Interest: The authors declare no conflicts of interest.

Abbreviations

I	mass moment of inertia	[kg·m ²]
M	load torque	[N·m]
N_0	rotational frequency	[min ⁻¹]
N	number of signal samples	[-]
$RMS M_D$	effective value of the dynamic component of the load torque	[N·m]
b	damping coefficient	[N·s·m ⁻¹]
f	frequency	[Hz]
i	gear ratio, harmonic component, number of cylinders	[-]
k	torsional stiffness	[N·m·rad ⁻¹]

n	RPM	$[\text{min}^{-1}]$
p	pressure	$[\text{kPa}]$
t	time	$[\text{s}]$
Ω_0	natural frequency	$[\text{rad}\cdot\text{s}^{-1}]$
γ	phase shift	$[\text{rad}]$
η	detuning coefficient	$[-]$
φ	angle of torsion, amplitude of rotation	$[\text{rad}]$
$\dot{\varphi}$	angular velocity	$[\text{rad}\cdot\text{s}^{-1}]$
$\ddot{\varphi}$	angular acceleration	$[\text{rad}\cdot\text{s}^{-1}]$
ω	angular frequency	$[\text{rad}\cdot\text{s}^{-1}]$

References

- Lu, J.; Zheng, H.; Husnain Haider, M.; Feng, Y.; Zhi, P.; Cheng, J.; Wang, Z. Fracture failure analysis of flywheel hub served in heavy-fuel aviation piston engine. *Eng. Fail. Anal.* **2023**, *151*, 107363. [\[CrossRef\]](#)
- Amiri, Z.; Bayatian, M.; Mozafari, S. Numerical simulation application in occupational health studies: A review. *Int. J. Occup. Saf. Ergon.* **2024**, *30*, 946–967. [\[CrossRef\]](#)
- Kassay, P. Effect of torsional vibration on woodchip size distribution. *Sci. J. Silesian Univ. Technol. Ser. Transp.* **2018**, *99*, 95–104. [\[CrossRef\]](#)
- Stanzl-Tschegg, S.E.; Mayer, H.R.; Tschegg, E.K. High frequency method for torsion fatigue testing. *Ultrasonics* **1993**, *31*, 275–280. [\[CrossRef\]](#)
- Czech, P. Diagnosing faults in the timing system of a passenger car spark ignition engine using the bayes classifier and entropy of vibration signals. *Sci. J. Silesian Univ. Technol. Ser. Transp.* **2022**, *116*, 83–98. [\[CrossRef\]](#)
- Henao, H.; Kia, S.H.; Capolino, G.-A. Torsional-Vibration Assessment and Gear-Fault Diagnosis in Railway Traction System. *IEEE Trans. Ind. Electron.* **2011**, *58*, 1707–1717. [\[CrossRef\]](#)
- Maláková, S.; Sivák, S. GPS Application in the Design of Gearboxes. *Acta Mech. Autom.* **2022**, *16*, 309–315. [\[CrossRef\]](#)
- Maláková, S.; Sivák, S. Practical Example of Modification of a Gearbox Lubrication System. *Lubricants* **2022**, *10*, 110. [\[CrossRef\]](#)
- Chmelař, J.; Petr, K.; Mossoczy, P.; Dynybyl, V. Experimental study of lubrication film monitoring in a roller bearing by utilization of surface acoustic waves. *Tribol. Int.* **2020**, *141*, 105908. [\[CrossRef\]](#)
- Chmelař, J.; Petr, K.; Mikeš, P.; Dynybyl, V. Cylindrical roller bearing lubrication regimes analysis at low speed and pure radial load. *Acta Polytech.* **2019**, *59*, 272–282. [\[CrossRef\]](#)
- Gładysiewicz, L.; Król, R.; Kisielewski, W. Measurements of loads on belt conveyor idlers operated in real conditions. *Meas. J. Int. Meas. Confed.* **2019**, *134*, 336–344. [\[CrossRef\]](#)
- dos Santos e Santos, L.; Ribeiro Filho, P.R.C.F.; Macêdo, E.N. Belt rotation in pipe conveyors: Development of an overlap monitoring system using digital twins, industrial Internet of things, and autoregressive language models. *Measurement* **2024**, *230*, 114546. [\[CrossRef\]](#)
- Urbanský, M.; Grega, R. Contactless Measuring Device for Flexible Shaft Coupling Twist Angle. In *Current Methods of Construction Design; Lecture Notes in Mechanical Engineering*; Springer: Cham, Switzerland, 2020; pp. 193–200, ISBN 9783030331450.
- Grega, R.; Krajnak, J.; Žul'ová, L.; Kačír, M.; Kaššay, P.; Urbanský, M. Innovative Solution of Torsional Vibration Reduction by Application of Pneumatic Tuner in Shipping Piston Devices. *J. Mar. Sci. Eng.* **2023**, *11*, 261. [\[CrossRef\]](#)
- Tuplin, W.A. LXV. Torsional vibration in certain mechanical systems. *Lond. Edinb. Dublin Philos. Mag. J. Sci.* **1938**, *26*, 729–752. [\[CrossRef\]](#)
- Pielorz, A. Vibration problems in selected torsional mechanical systems. *Meccanica* **2003**, *38*, 731–738. [\[CrossRef\]](#)
- Chen, X.; Chen, R.; Deng, T. An investigation on lateral and torsional coupled vibrations of high power density PMSM rotor caused by electromagnetic excitation. *Nonlinear Dyn.* **2020**, *99*, 1975–1988. [\[CrossRef\]](#)
- Homik, W.; Mazurkow, A.; Woś, P. Application of a Thermo-Hydrodynamic Model of a Viscous Torsional Vibration Damper to Determining Its Operating Temperature in a Steady State. *Materials* **2021**, *14*, 5234. [\[CrossRef\]](#)
- Guo, Y.; Li, W.; Yu, S.; Han, X.; Yuan, Y.; Wang, Z.; Ma, X. Diesel engine torsional vibration control coupling with speed control system. *Mech. Syst. Signal Process* **2017**, *94*, 1–13. [\[CrossRef\]](#)
- Kinnunen, K.; Laine, S.; Tiainen, T.; Viitala, R. Method for Adjusting Torsional Natural Frequencies of Powertrains with Novel Coupling Design. *Machines* **2022**, *10*, 162. [\[CrossRef\]](#)
- Wieczorek, A.N.; Konieczny, Ł.; Wojnar, G.; Wyroba, R.; Filipowicz, K.; Kuczaj, M. Reduction of dynamic loads in the drive system of mining scraper conveyors through the use of an innovative highly flexible metal coupling. *Eksploat. I Niezawodn. Maint. Reliab.* **2024**, *26*, 181171. [\[CrossRef\]](#)
- Urbanský, M. Comparison of piston and tangential pneumatic flexible shaft couplings in terms of high flexibility. *Sci. J. Silesian Univ. Technol. Ser. Transp.* **2018**, *99*, 193–203. [\[CrossRef\]](#)
- Laine, S.; Haikonen, S.; Tiainen, T.; Viitala, R. Rotor resonance avoidance by continuous adjustment of support stiffness. *Int. J. Mech. Sci.* **2024**, *270*, 109092. [\[CrossRef\]](#)

24. Flek, J.; Dub, M.; Kolář, J.; Lopot, F.; Petr, K. Determination of Mesh Stiffness of Gear—Analytical Approach vs. FEM Analysis. *Appl. Sci.* **2021**, *11*, 4960. [CrossRef]
25. Li, W.; Ge, X.; Liang, M.; Deng, X. Magneto-rheological variable damping and variable stiffness torsional vibration control of powertrain transmission. *J. Mech. Sci. Technol.* **2023**, *37*, 3887–3900. [CrossRef]
26. Zhang, X.; He, W.; Hu, J. Impact of Inertia Control of DFIG-Based WT on Torsional Vibration in Drivetrain. *IEEE Trans. Sustain. Energy* **2020**, *11*, 2525–2534. [CrossRef]
27. Homišin, J. *New Types of Flexible Shaft Couplings: Development, Research, Application*; Vienala: Košice, Slovakia, 2002. Available online: https://scholar.google.sk/scholar?cluster=17005307171049548256&hl=en&as_sdt=2005&scioldt=0,5 (accessed on 31 October 2024). (In Slovak)
28. Homišin, J. Optimal tuning of mechanical systems by application of a pneumatic tuner of torsional oscillation. *Sci. J. Silesian Univ. Technol. Ser. Transp.* **2017**, *97*, 47–55. [CrossRef]
29. Bartel, T.; Herold, S.; Infante, F.; Käsgen, J.; Matthias, M.; Millitzer, J.; Perfetto, S. Active Vibration Reduction of Ship Propulsion Systems. In Proceedings of the 2018 Joint Conference—Acoustics, Acoustics 2018, Ustka, Poland, 11–14 September 2018; Polish Acoustical Society: Gdańsk, Poland; Ustka, Poland, 2018; pp. 15–20.
30. Xingyu, L.; Gequn, S.; Lihui, D.; Bin, W.; Kang, Y. Progress and Recent Trends in the Torsional Vibration of Internal Combustion Engine. In *Advances in Vibration Analysis Research*; Ebrahimi, F., Ed.; InTech: Rijeka, Croatia, 2011; pp. 245–272, ISBN 978-953-307-209-8.
31. Kongratana, V.; Tipsuwanporn, V.; Numsomran, A.; Detchrat, A. IMC-based PID controllers design for torsional vibration system. In Proceedings of the 2012 12th International Conference on Control, Automation and Systems, Jeju, Republic of Korea, 17–21 October 2012; pp. 892–895.
32. Zhong, B.; Deng, B.; Zhao, H. Simulation Model and Method for Active Torsional Vibration Control of an HEV. *Appl. Sci.* **2019**, *9*, 34. [CrossRef]
33. Homišin, J.; Kaššay, P.; Urbanský, M. High-flexibility characteristics of pneumatic flexible shaft couplings. *Pneumatyka* **2011**, *79*, 26–29.
34. Kaššay, P.; Urbanský, M. Torsional natural frequency tuning by means of pneumatic flexible shaft couplings. *Sci. J. Silesian Univ. Technol. Ser. Transp.* **2015**, *89*, 57–60. [CrossRef]
35. Jírová, R.; Pešík, L.; Grega, R. An Original Vibrodiagnostic Device to Control Linear Rolling Conveyor Reliability. *J. Mar. Sci. Eng.* **2022**, *10*, 445. [CrossRef]
36. Bruha, M. Importance of control engineering to minimize torsional vibration in variable speed drive systems. In Proceedings of the 2016 Petroleum and Chemical Industry Conference Europe Conference Proceedings, PCIC EUROPE, Berlin, Germany, 14–16 June 2016; pp. 1–8. [CrossRef]
37. Homišin, J. Static optimisation of mechanical systems based on the method of extremal regulation. *Sci. J. Silesian Univ. Technol. Ser. Transp.* **2019**, *103*, 15–29. [CrossRef]
38. Naqvi, S.; Ghufuran, M.; Meraghni, S.; Varnier, C.; Nicod, J.; Zerhouni, N. Human knowledge centered maintenance decision support in digital twin environment. *J. Manuf. Syst.* **2022**, *65*, 528–537. [CrossRef]
39. Xia, M.; Shao, H.; Williams, D.; Lu, S.; Shu, L.; Silva, C.W. Intelligent fault diagnosis of machinery using digital twin-assisted deep transfer learning. *Reliab. Eng. Syst. Saf.* **2021**, *215*, 107938. [CrossRef]
40. Wang, H.; Liu, Y.; Mu, Z.; Xiang, J.; Li, J. Real-time precision reliability prediction for the worm drive system supported by digital twins. *Reliab. Eng. Syst. Saf.* **2023**, *240*, 109589. [CrossRef]
41. Zoul, V. Dynamic of propulsion, present situation and trends. *Trans. Univ. Košice* **2014**, *2*, 101–106.
42. Rivin, E.I. *Dinamika Privoda Stankov*; Mašinstrojenje: Moskva, Russia, 1966. (In Russian)
43. Urbanský, M.; Homišin, J.; Kaššay, P.; Moravič, M. Influence of Piston Compressor Inner Failure on Mechanical System Objective Function. *Diagnostyka* **2016**, *17*, 47–52.
44. Chen, M.; Ouyang, H.; Li, W.; Wang, D.; Liu, S. Partial Frequency Assignment for Torsional Vibration Control of Complex Marine Propulsion Shafting Systems. *Appl. Sci.* **2020**, *10*, 147. [CrossRef]
45. Wachel, J.C.; Szenasi, F.R. Analysis of Torsional Vibrations in Rotating Machinery. In Proceedings of the Twenty-Second Turbomachinery Symposium, Dallas, TX, USA, 14–16 September 1993; Texas A&M University: College Station, TX, USA, 1993; pp. 127–151.
46. Harris, C.M.; Piersol, A.G. *Harris' Shock and Vibration Handbook*, 5th ed.; McGraw-Hill Handbooks: New York, NY, USA, 2002.
47. Wilson, W.K. *Practical Solution of Torsional Vibration Problems: Frequency Calculations*, 3rd ed.; Chapman & Hall Ltd.: London, UK, 1967; Volume 1.
48. Wilson, W.K. *Practical Solution of Torsional Vibration Problems: Amplitude Calculations*, 3rd ed.; Chapman & Hall Ltd.: London, UK, 1963; Volume 2.
49. Ding, H.; Dong, Y.; Zhang, Y.; Wen, C.; Yang, Y. Performance of supercritical carbon dioxide (sCO₂) centrifugal compressors in the Brayton cycle considering non-equilibrium condensation and exergy efficiency. *Energy Convers. Manag.* **2024**, *299*, 117849. [CrossRef]

50. Zhang, G.; Yang, Y.; Chen, J.; Jin, Z.; Majkut, M.; Smolka, K.; Dykas, S. Effect of relative humidity on the nozzle performance in non-equilibrium condensing flows for improving the compressed air energy storage technology. *Energy* **2023**, *280*, 128240. [[CrossRef](#)]
51. Zhang, G.; Yang, Y.; Chen, J.; Jin, Z.; Dykas, S. Numerical study of heterogeneous condensation in the de Laval nozzle to guide the compressor performance optimization in a compressed air energy storage system. *Appl. Energy* **2024**, *356*, 122361. [[CrossRef](#)]

Disclaimer/Publisher's Note: The statements, opinions and data contained in all publications are solely those of the individual author(s) and contributor(s) and not of MDPI and/or the editor(s). MDPI and/or the editor(s) disclaim responsibility for any injury to people or property resulting from any ideas, methods, instructions or products referred to in the content.